journal of the mechanical behavior of biomedical materials 148 (2023) 106195

Contents lists available at ScienceDirect

Journal of the Mechanical Behavior of Biomedical Materials

journal homepage: www.elsevier.com/locate/jmbbm

Depth profiling via nanoindentation for characterisation of the elastic modulus and hydraulic properties of thin hydrogel layers

Dichu Xu [a,b,*], Maria Luisa Hernandez Miranda [c], Nicholas D. Evans [b,c], Bram G. Sengers [b], Martin Browne [b], Richard B. Cook [a]

[a] National Centre for Advanced Tribology at Southampton (nCATS), University of Southampton, Southampton, UK
[b] Bioengineering Science Research Group, University of Southampton, Southampton, UK
[c] Bone and Joint Research Group, Centre for Human Development, Stem Cells and Regeneration, Faculty of Medicine, University of Southampton, Southampton General Hospital, Southampton, UK

ARTICLE INFO

Keywords:
Nanoindentation
Hydrogel thickness
Elastic modulus
Permeability

ABSTRACT

The accurate determination of the mechanical properties of hydrogels is of fundamental importance for a range of applications, including in assessing the effect of stiffness on cell behaviour. This is a particular issue when using thin hydrogel layers adherent to stiff substrate supports, as the apparent stiffness can be significantly influenced by the constraint of the underlying impermeable substrate, leading to inaccurate measurements of the elastic modulus and permeability of thin hydrogel layers. This study used depth profiling nanoindentation and a poroelastic model for spherical indentation to identify the elastic moduli and hydraulic conductivity of thin polyacrylamide (PAAm) hydrogel layers (~27 μm–782 μm thick) on impermeable substrates. The apparent stiffness of thin PAAm layers increased with indentation depth and was significantly greater than those of thicker hydrogels, which showed no influence of indentation depth. The hydraulic conductivity decreased as the geometrical confinement of hydrogels increased, indicating that the fluid became more constrained within the confinement areas. The impact of geometrical confinement on the apparent modulus and hydraulic conductivity of thin PAAm hydrogel layers was then established, and their elastic moduli and intrinsic permeability were determined in relation to this effect. This study offers valuable insights into the mechanical characterisation of thin PAAm hydrogel layers used for the fundamental study of cell mechanobiology.

1. Introduction

Hydrogels can model physical properties of the extracellular matrix, such as the stiffness and porosity, through precise control of the chemical composition, and have found promise in various applications, such as cell culture, drug delivery system, and hydrophilic coatings on biomedical implants (Cushing and Anseth, 2007; Li and Mooney, 2016; Fu et al., 2021). The mechanical properties of hydrogel matrices, either alone or coupled with their structural or compositional properties, can drastically alter cell activities (Buxboim et al., 2010), cell function (Nicodemus and Bryant, 2008), and cell fate or differentiation (Chaudhuri et al., 2016; Tsou et al., 2016). Polyacrylamide (PAAm) hydrogels are frequently used as cell culture platforms for the study of cellular mechanobiology (Pelham et al., 1997), because the elastic modulus and porosity of PAAm can be easily controlled by adjusting the ratios of monomer to the cross-linker. Cell adhesion can be facilitated by covalently crosslinking small matrix proteins to the surface, and in this manner, these materials have been used to show that stiffness correlates with cell differentiation (Engler et al., 2006).

Cells sense hydrogel stiffness by exerting forces on the surface of the hydrogels to which they are adhered and by detecting the dynamic displacements that are induced (Pelham et al., 1997; Munevar et al., 2001; Evans et al., 2009; Evans and Gentleman, 2014). These displacements occur at the length scale of cells or groups of cells, on the order of tens to hundreds of microns (Tusan et al., 2018; Trepat et al., 2009), and so testing methods should reflect these length scales. This is particularly important where hydrogel geometry is concerned, as it has been shown that cells or groups of cells can 'feel through' thin hydrogels (Buxboim et al., 2010; Tusan et al., 2018; Hernandez Miranda, 2023). This becomes important where cell-induced displacements become large relative to the thickness of the hydrogel, which is dependent on the magnitude of the forces the cells exert (Hernandez-Miranda et al., 2023).

* Corresponding author. National Centre for Advanced Tribology at Southampton (nCATS), University of Southampton, Southampton, SO17 1BJ, UK.
E-mail address: D.Xu@soton.ac.uk (D. Xu).

https://doi.org/10.1016/j.jmbbm.2023.106195
Received 5 September 2023; Received in revised form 10 October 2023; Accepted 13 October 2023
Available online 14 October 2023

This is particularly important for PAAm hydrogels, as they are usually fabricated as gel layers tens to hundreds of microns thick covalently coupled to an underlying glass support for ease of handling (Hernandez-Miranda et al., 2023). Here, the displacements caused by the cells might be restricted by the proximity of the underlying support, and the hydrogel's geometry plays a substantial role in influencing the accuracy of mechanical characterisation for PAAm hydrogel layers.

However, the accurate determination of the mechanical properties of thin PAAm hydrogels layers is still challenging, as most conventional testing methods lack a good spatial resolution for characterising thin hydrogel layers tens to hundreds of microns thick adherent to stiff substrate supports (Rice and Anseth, 2004; Qian and Zhao, 2018; Cao et al., 2019; Cha et al., 2010; Huang et al., 2018). In contrast to macroscopic methods, instrumented nanoindentation has the capability of quantitatively analysing soft materials at testing length scales varying from submicron/nanometre to micron range, with elastic moduli ranging from single kilopascals (kPa) to megapascals (MPa), while also being able to differentiate between poroelastic and viscoelastic time dependent behaviour (Kalcioglu et al., 2012; Islam and Oyen, 2021).

However, the elastic moduli of thin hydrogel layers characterised by nanoindentation can be greatly influenced by the underlying substrate, as the measured values of the elastic moduli represent a combination of the soft film and the stiff substrate due to the interaction volume during indentation. Previous studies (Bückle, 1965; Manika and Maniks, 2008; Chen and Bull, 2009) have suggested that the elastic moduli might not be affected by the stiff substrate when the indentation depth is less than a predefined threshold value (e.g. 10% of the film thickness according to Bückle's rule (Bückle, 1965)). Nevertheless, it is important to note that the threshold value can vary depending on the specific combinations of coatings and substrates, as well as the test conditions (Clifford and Seah, 2006a). Consequently, previous models have yielded disparate predictions regarding the effects of the substrate on soft gels (Clifford and Seah, 2006a, 2009; Dimitriadis et al., 2002; Hu et al., 2011). Hence, a more rigorous approach would involve decoupling the elastic moduli of soft films and stiffer substrates using analytical models. These models should be further validated through experiments, particularly focusing on soft hydrogels with elastic moduli ranging from 1 to 100 kPa.

Moreover, hydrated materials such as hydrogels consist of water within a three-dimensional network of covalently crosslinked polymer chains, and consequently the mechanical response of the gel is strongly dependent on both the elastic properties of the hydrogel skeleton and the time-dependent water movement through the deformed gels, i.e., poroelasticity, which may have influence on the growth and morphology of cells (Asp et al., 2022). Therefore, the accurate mechanical characterisation of thin hydrogel layers faces additional complexity due to their poroelastic behaviour, which can exhibit variations at different length scales. This is attributed to the presence of an impermeable underlying substrate, creating a confined region beneath the indenter that hinders fluid flow out of the deformed gels (Delavoipière et al., 2016; Galli and Oyen, 2008). Consequently, a higher hydrostatic pressure builds up beneath the indenter compared to that within an unconfined layer. As a result, the predicted elastic moduli of confined hydrated gels can be significantly overestimated (Degen et al., 2020).

To characterise the poroelasticity of hydrated materials, Oyen (Oyen et al., 2006; Oyen, 2008) and co-workers (Galli and Oyen, 2009) developed a master curve method for the identification of poroelastic parameters via indentation tests coupled with finite element (FE) modelling for hydrated materials. Later, the master curve method was further extended to characterise finite poroelastic coatings (Galli and Oyen, 2008). Compared with the ramp-hold creep indentation tests carried out by Oyen et al., Hu et al. (Hu et al., 2010, 2011; Chan et al., 2012a, 2012b) utilised the force relaxation curves from spherical indentation tests to characterise the poroelasticity of the gels. Degen et al. (2020) used this to quantify the influence of fluid flow on the apparent stiffness of highly confined hydrogel layers, in which the Winkler foundation model (Chau et al., 2021) was applied to characterise the elastic modulus of the fully drained polymer network. As the Winkler foundation model predicts a lower spring constant/stiffness at a large indentation depth, the influence of the fluid flow confinement on the apparent stiffness can be overestimated.

The objective of this study is to introduce a novel and straightforward method for characterising the poroelasticity (elastic moduli and hydraulic conductivity) of thin, soft gel layers using spherical nanoindentation and analytical models, when taking into consideration the effects of the underlying impermeable substrate. PAAm hydrogels are fabricated as model systems with two levels of polymer concentration, as well as four levels of hydrogel thickness ranging from tens to hundreds of μm. Depth profiling is conducted on gel layers with different thicknesses to identify the effect of the substrate. A poroelastic model is developed to describe the relationship between the displacement rate and hydraulic pressure build-up by fluid migration through the compressed region of the fluid-filled gel layers during the holding period of indentation, for both unconfined and geometrically confined conditions.

2. Methods

2.1. Material synthesis

PAAm hydrogels of defined thicknesses suitable for cell culture were formed on 13 mm diameter coverslips (VWR international, Leicestershire, UK) as in previous studies (Pelham et al., 1997; Tusan et al., 2018). To covalently bond to the PAAm gels, the coverslips were first cleaned and activated by dripping 200 μL of 0.2 M NaOH on the coverslip surface until evaporation was completed on a hotplate at 80 °C. Coverslips were then thoroughly washed in deionised H_2O and dried before addition of 125 μL APES (3-Aminopropyltriethoxysilane; Sigma-Aldrich) and incubated for 5 min at room temperature. Coverslips were further washed and incubated for 30 min in a well-plate containing 0.5% (v/v) gluteraldehyde (Sigma-Aldrich) in phosphate-buffered saline (PBS; Sigma-Aldrich) at room temperature, rinsed and dried.

PAAm was polymerised from constituent monomer (acrylamide) and a crosslinker (bisacrylamide) *in situ*. For low elastic modulus hydrogels, acrylamide and N,N′-Methylenebisacrylamide (bis) were mixed at volumes of 15% (v/v) acylamide and 1.5% (v/v) bis; for high elastic modulus hydrogels these reagents were mixed at 20% (v/v) acrylamide and 24% (v/v) bis, both in PBS to a final volume of 1 mL and degassed. To initiate polymerisation, 1 μL of N,N,N′,N′ tetramethylethylenediamine (Sigma-Aldrich) and 10 μL of 10% (w/v) $(NH_4)_2S_2O$ (Sigma-Aldrich) were added and the solution briefly vortexed. This solution was immediately pipetted at volumes of 5, 25, 50 or 100 μL onto the surface of hydrophobic glass slides (pre-treated with dichlorodimethylsilane for 5 min, washed and polished with a lint-free tissue). The treated coverslips, prepared as above, were then immediately placed on to the pipetted droplets with the functionalised surface downwards, to sandwich a layer of polymerising gel between the hydrophobic glass slide and the functionalised coverslip. Once polymerised (after 30 min at room temperature), glass slide/coverslips were immersed in PBS for 10 min at room temperature to hydrate before careful detachment of the coverslip-adhered PAAm from the dichlorodimethylsilane-treated slides using a scalpel blade. The coverslips with the adhered gels were placed in plastic 24-well plates containing 1 mL PBS and washed overnight on an orbital shaker at 4 °C to remove free monomer. For covalent attachment of collagen to gel surfaces, hydrogels were covered with 125 μL of 0.5 mg/mL sulfosuccinimidyl 6-(4′-azido-2′-nitrophenylamino) hexanoate (Sulfo-SANPAH; ThermoFisher Scientific) in 50 mM 4-(2-Hydroxyethyl)piperazine-1-ethanesulfonic acid pH 8.5 (HEPES, Sigma-Aldrich) and irradiated with UV light for 25 min using a UV transilluminator (Chromatovue TM-20, UVP transilluminator, 240 V). Hydrogels were then washed three times with HEPES and incubated overnight with 1 mL of a solution of 0.1 mg/mL collagen in HEPES buffer (CellSystems Biotechnologie) 4 °C on an orbital shaker.

To enable thickness measurement using confocal microscopy, 0.2% allylamine (v/v, Sigma-Aldrich) was added to the solution before polymerisation to allow dye binding. Once polymerised, the gels were incubated in Alexa Fluor™ 488 NHS Ester (1 mg/mL) diluted in PBS for 3 h at room temperature in the dark for staining.

After washing three times with PBS, the average thickness of the PAAm hydrogel samples was measured by confocal microscopy (Leica, SP8) prior to nanoindentation testing. The fluorescent intensity was measured at 20X magnification, using 2 μm z-stacks from the top to the bottom of the gels (Table 1). The measurements were quantified in three hydrogel triplicates at each condition, and the standard deviation corresponds to those three measurements in each case.

2.2. Nanoindentation

Nanoindentation experiments were performed on the PAAm hydrogel specimen utilising the soft contact protocol of the NanoTest Vantage system (MicroMaterials Ltd., Wrexham). Full details of the soft contact testing protocol have been described in the authors' previous work (Xu et al., 2022).

Two samples of each combination of PAAm composition and thickness were tested using a 500 μm radius spherical diamond tip, while fully immersed in PBS solution. To obtain the indentation (or reduced) modulus (E_r) vs. depth (δ) profile, the nanoindentation tests were performed in load control to differing maximum loads (ranging from 10 μN to 850 μN with a minimum load step of 2 μN), providing a range of indentation depth/hydrogel thickness ratios (δ/h) between 0.01 and 0.5, with all indents spaced 250 μm apart. For all the tests, a hold period of 120 s at maximum load was applied before unloading. The loading and unloading rates were set at 1 μN/s and 5 μN/s, respectively. All tests were run in a temperature-controlled environment (20 ± 1 °C).

2.3. Statistical quantification

In order to identify if there was a statistically significant difference between the two groups, a one-way ANOVA with Tukey's HSD post hoc test was employed (Pereira et al., 2015). Statistical significance was achieved when p-values were less than 0.05.

3. Poroelastic analysis

3.1. Elastic and creep analysis

The force-displacement data can be fitted to the Hertzian elastic loading response for a spherical tip with a radius of R, as expressed in Equation (1) (Swain et al., 2017; Kontomaris and Malamou, 2020)

$$F_e = \frac{4}{3}E^* R^{1/2}\delta^{3/2} \tag{1}$$

where F_e is the elastic load response, δ is the displacement. E^* denotes the apparent or loading effective modulus (Swain et al., 2017). The Hertz model applied for soft biomaterials with several assumptions. Firstly, the samples can be regarded as isotropic and homogeneous materials. Secondly, it is assumed that there is no adhesion and friction between the contacting surfaces. Thirdly, the sample can be considered as an infinite half space, which means the sample thickness is much larger in comparison to other length scales (e.g. the indenter radius or contact depth) (Kontomaris and Malamou, 2020; Long et al., 2011).

Table 1
Average thicknesses of PAAm hydrogel specimens.

PA mixture volume (μL)	Average thickness (μm)	
	Low Concentration (12.5% v/v) of AAm	High concentration (20% v/v) of AAm
5	54.53 ± 5.74	27.44 ± 1.59
25	308.91 ± 15.55	214.94 ± 52.56
50	596.72 ± 15.78	276.69 ± 25.17
100	781.67 ± 64.93	555.49 ± 49.22

According to the Biot's theory (Biot, 1955), the normal force (F) induced by the indenter pressing a fluid filled film consists of two components, the elastic portion related to the elastic modulus of the polymer network skeleton, and the time-dependent portion related to the permeability of the porous network (Equation (2))

$$F = F_p + \frac{4}{3}E_{er}R^{1/2}\delta^{3/2} \tag{2}$$

Where, the term F_p is the time-dependent portion which reaches zero in the final equilibrium state when $d\delta/dt = 0$. By fitting the displacement curves using the empirical creep function $\delta(t) = \delta(0) - A_0\exp(-t/\tau)$ (Oyen, 2005) and extrapolating to the time when the displacement rate $d\delta/dt \to 0$, the maximum indentation depth δ_∞ can be estimated, and subsequently used to determine the equilibrium reduced modulus E_{er}. The reduced modulus $E_r = E_s/(1-\upsilon_s^2)$ where E_s is the Young's modulus of the specimen, and υ_s is the Poisson's ratio of the specimen. The reduced modulus will be reported in this study instead of the Young's modulus as the actual values of the Poisson's ratio for these hydrogels were not known, and would have varied with the gel composition.

Then, the displacement rate ($d\delta/dt$) or the normalised displacement rate ($\dot{\Delta}_c = \left(\frac{\delta}{h} - \frac{\delta}{h_\infty}\right)/\left(\frac{\delta}{h_0} - \frac{\delta}{h_\infty}\right)$) can also be calculated, by fitting the curves up to the end of the hold period of 120s, and then extrapolating the displacement rate beyond 120s until $d\delta/dt \to 0$. The time t is normalised with the sample size as the normalised creep time $t_n = t/(R\delta)$. In this study, the term 'creep' denotes the displacement during the hold period of the indentation test.

To account for the substrate effect on the reduced moduli of finite hydrogel layers, Equation (2) was further modified by introducing a correction factor, given by Equation (3) (Degen et al., 2020)

$$F = F_p + \frac{4}{3}E_{er,c}R^{1/2}\delta^{3/2}\cdot f(\alpha) \tag{3}$$

where $f(\alpha)$ denotes the correction factor which is a measure of substrate effect, $E_{er,c}$ denotes the corrected equilibrium reduced modulus by considering the substrate effect on the reduced modulus. This correction factor is related with a dimensionless number $\alpha = \sqrt{R\delta}/h$ (where h denotes the thickness of hydrogel layer) which describes the level of the geometrical confinement (Degen et al., 2020).

3.2. Poroelastic analysis on a thick hydrogel layer

For the thick hydrogel (Fig. 1a), the radius of the contact area is much less than the thickness of the hydrogel ($\sqrt{R\delta} < h$). Based on Darcy's law, the poroelastic response (F_p) in Equation (3) can be given by the analytical solution previously developed by Swain et al. (2017).

According to Darcy's law (Swain et al., 2017; Bear, 1988), the flow of the fluid (Q) through a porous network is related to the pressure (p), as expressed in Equation (4)

$$Q = \frac{KpA}{L} \tag{4}$$

Where K is the hydraulic conductivity (also known as Darcy's permeability) and the intrinsic permeability $\kappa = \eta\cdot K$ (η is the viscosity of the fluid, $\eta = 0.8872$ mPa s for PBS solution at 20 °C). A is the area of the structure under pressure and L the distance through which the fluid flows.

As the spherical indenter is pressed into a fluid filled gel, the volume of the fluid (V) displaced can be estimated as $V = \pi\delta^2\left(R + \frac{\delta}{6}\right)$ or $\pi R\delta^2$ ($\delta \ll R$) (Swain et al., 2017). Then, the flow rate in Equation (4) can also be expressed in Equation (5) as

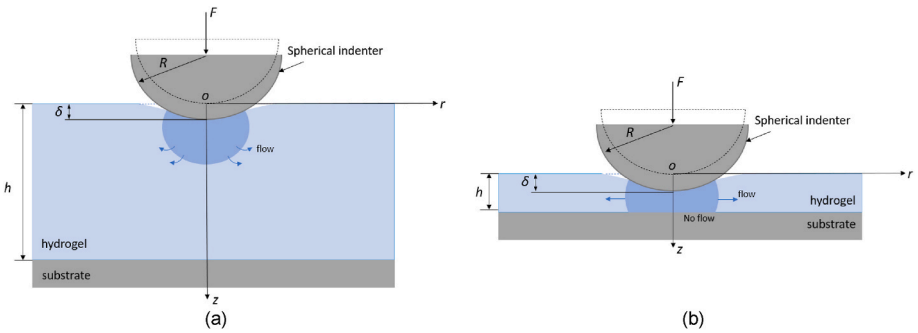

Fig. 1. The fluid migration within the deformed region of hydrogel layers when pressed by the indenter: (a) unconfined condition; (b) geometrically confined condition; adapted from Ref (Chan et al., 2012b).

$$Q = \frac{dV}{dt} = \frac{dV}{dh}\frac{dh}{dt} = 2\pi R\delta\frac{dh}{dt} \tag{5}$$

There is a spherical volume beneath the spherical indenter where the fluid migration occurs, and the dimension L scales with the radius of this spherical volume which approximates to $\sqrt{2R\delta}$ (Galli and Oyen, 2009; Swain et al., 2017). The term pA denotes the force F_p, so combining Equations (4) and (5) yields

$$F_p = \pi\frac{(2R\delta)^{3/2}}{K}\frac{d\delta}{dt} \tag{6}$$

3.3. Poro-elastic analysis on a thin hydrogel layer

For a thin hydrogel layer on a stiff impermeable substrate (Fig. 1b), the contact radius a would be larger than the hydrogel thickness ($\sqrt{R\delta} \geq h$). The volume of fluid migration beneath the indenter would be squashed into an approximate cylindrical shape due to geometric confinement (Chan et al., 2012c), and thus, the total fluid flow displaced by the indenter can be evaluated in Equation (7)

$$Q = \int_0^{\sqrt{2R\delta}} dr\cdot(2\pi r)\cdot\frac{d\delta}{dt} = 2\pi(R\delta)\frac{d\delta}{dt} \tag{7}$$

In addition, the radial fluid flow through the cylindrical volume is given by Darcy's law (Equation (8))

$$Q = K\frac{p}{l}\cdot 2\pi l\cdot(h-\delta) \tag{8}$$

Combining Equations (7) and (8), the pore pressure (p_0) build-up in the centre is obtained (Equation (9))

$$p_0 = \frac{R\delta}{K(h-\delta)}\cdot\frac{d\delta}{dt} \tag{9}$$

The pore pressure distribution beneath the indenter can be written as a parabolic distribution profile (Delavoipière et al., 2016) (Equation (10))

$$p_r = p_0\left(1 - r^2/l^2\right) \tag{10}$$

where p_0 is the maximum pressure, and the channel length l scales with the radius of the cylinder volume ($\sim\sqrt{2R\delta}$) [37,44]; combining Equations (9) and (10) yields

$$F_p = \int_0^{\sqrt{2R\delta}} p_r\cdot 2\pi r\cdot dr = \frac{\pi(R\delta)^2}{K(h-\delta)}\frac{d\delta}{dt} \tag{11}$$

Therefore, based on Equations (3), (6) and (11), the displacement rates at the constant load during the hold period can be expressed for unconfined ($\sqrt{R\delta} < h$) as

$$\frac{d\delta}{dt} = \frac{F - \frac{4}{3}E_{er}R^{1/2}\delta^{3/2}}{(\pi/K)(2R\delta)^{3/2}} \tag{12}$$

and for confined gels ($\sqrt{R\delta} \geq h$) as,

$$\frac{d\delta}{dt} = \frac{F - \frac{4}{3}E_{er}R^{1/2}\delta^{3/2}}{\pi(R\delta)^2/(K(h-\delta))} \tag{13}$$

respectively. Once the elastic resistance of the gels (F_e) was solved, the hydraulic conductivity (Darcy's permeability) K could be determined by fitting the displacement rate during the hold period of the indentation to Equations (12) and (13) for unconfined and confined gels, respectively.

4. Results

4.1. Effect of indentation depth (δ) and gel thickness on equilibrium reduced modulus

The E_{er} values overlapped and were independent of δ for the 309, 597 and 782 μm thick 12.5% PAAm gels and the 277 and 555 μm thick 20% PAAm gels (Fig. 2). The average E_{er} values from the overlapped data set were 6.95 ± 2.63 kPa and 69.4 ± 9.66 kPa for the 12.5% and 20% PAAm gels respectively, with significant differences found between the two data sets ($p < 0.001$). The E_{er} values for the 215 μm thick 20% PAAm layer were slightly higher than the average values for thick 277 μm and 555 μm 20% PAAm gels (Fig. 2b).

The E_{er} values obtained from the thinnest PAAm samples (55 μm thick 12.5% PAAm gels and 27 μm thick 20% PAAm gels) were much higher than the averaged values for thicker layers and showed a dependence of E_{er} values on δ (Fig. 2). The E_{er} values increased consistently with δ for the 27 μm 20% PAAm gels, with a linear regression model fitting to the nanoindentation measurements (Fig. 2b). In contrast, the 55 μm thick 12.5% PAAm gel exhibited no increase in E_{er} values up to $\delta \sim 10$ μm, after which they exponentially increased (Fig. 2a).

The equilibrium reduced modulus E_{er} values for 782 μm thick 12.5% PAAm gels and 555 μm thick 20% PAAm gels were independent of indentation depth and can be determined by the averaged values (noted as E_b) indicated by the dotted horizontal lines in Fig. 2. Normalised modulus values (E_{er}/E_b) were obtained for both 12.5% and 20% PAAm gels and plotted against α ($\alpha = \sqrt{R\delta}/h$) for comparison against the theoretical models used in previous studies (Dimitriadis et al., 2002; Hu et al., 2011) (Fig. 3). The data was found to overlay for PAAm gels with different polymer concentrations and layer thicknesses. An empirical analytical curve was found to best fit the nanoindentation data with the function of $E_{er}/E_b = \exp(0.9049\cdot\alpha)$, between the predictions of previous analytical models.

The averaged apparent modulus (E^*) obtained by Hertzian model based on Equation (1), the equilibrium reduced modulus (E_{er})

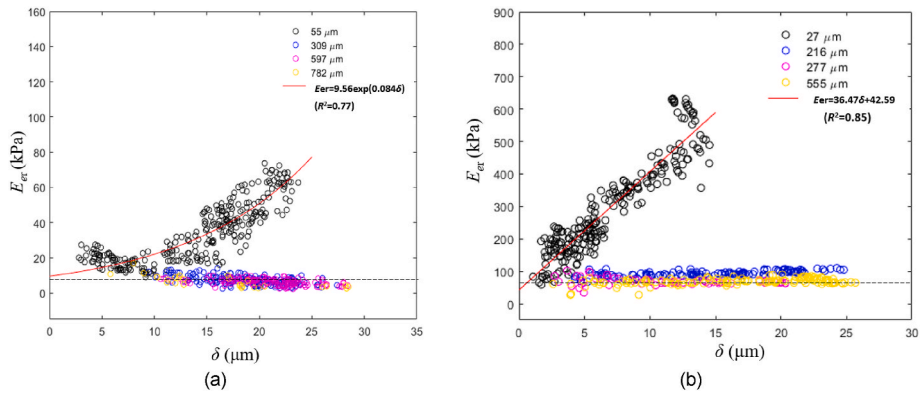

Fig. 2. The equilibrium reduced modulus E_{er} values as a function of indentation depth δ for PAAm layers with different layer thickness: (a) 12.5% PAAm hydrogels (b) 20% PAAm hydrogels.

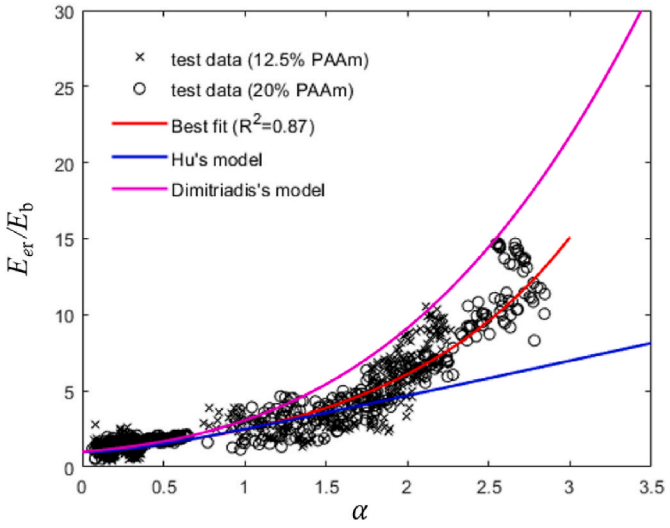

Fig. 3. Normalised reduced modulus values as a function of dimensionless number α, compared with Dimitriadis et al.'s (Dimitriadis et al., 2002) and Hu et al.'s (Hu et al., 2011) analytical models.

considering the poroelastic effect but without considering the substrate effect, and the corrected equilibrium elastic modulus ($E_{er,c}$) using the empirical function $E_{er}/E_b = \exp(0.9049 \cdot \alpha)$ which considers both the poroelastic and the substrate effects, were replotted against the layer thickness for 12.5% and 25% PAAm, respectively (Fig. 4).

The E^* values were higher than E_{er} values with larger discrepancies. The E^* and E_{er} values exponentially decreased with gel thickness. Much higher modulus values with larger standard deviations were found in the E^* and E_{er} values for thin gel layers, with significant differences found between the two groups of 12.5% PAAm gels with thickness below 600 μm ($p < 0.001$, Fig. 4a), and between the groups of 20% PAAm gels with thickness below 277 μm ($p < 0.001$, Fig. 4b). No significant difference was found in the E^* values with the gel thickness >600 μm for the 12.5% PAAm, while the E^* values were still found significantly different with the gel thickness >277 μm for the 20% PAAm.

The E_{er} values reached a steady state when the gel thickness >600 μm for 12.5% PAAm and >277 μm for 20% PAAm respectively, with no significant difference found between the E_{er} values for the samples with different gel thickness but the same composition ($p > 0.05$). The corrected values ($E_{er,c}$) for the samples with different thickness but the same gel composition were very similar with no significant difference between the $E_{er,c}$ values ($p > 0.05$), and fitted a horizontal line.

4.2. *Effects of indentation depth and gel thickness on the displacement rate during the hold period*

The typical creep response due to poroelastic flow for the 20% PAAm hydrogels of 27 μm thickness is shown in Fig. 5. The normalised displacement rate ($\dot{\Delta}_c$) at a range of indentation depths for 20% PAAm hydrogels of 27, 215, 277, 550 μm thickness were plotted against creep time t and normalised creep time $t/(R\delta)$ in Figs. 6 and 7, respectively. The curves of $\dot{\Delta}_c$ showed an exponential decay, with the shape of the curve $\dot{\Delta}_c$ vs. t strongly dependent on δ. As δ increased, the displacement relaxation rate was reduced. In contrast, the curve of $\dot{\Delta}_c$ vs. $t/(R\delta)$ is

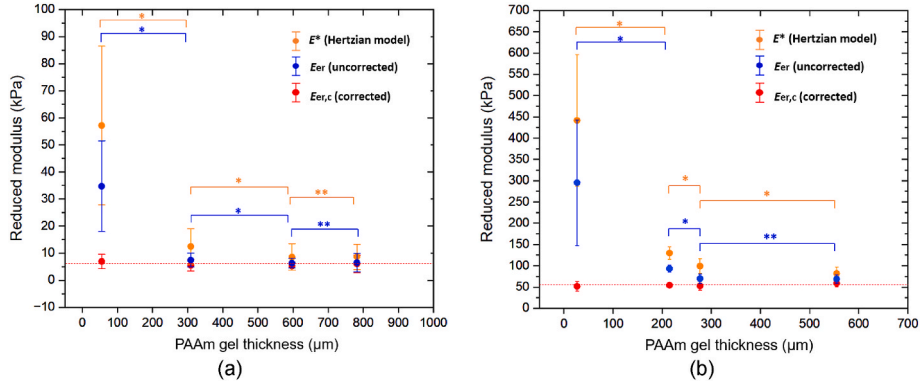

Fig. 4. The averaged apparent modulus E^* values given by the Hertzian model and equilibrium reduced modulus E_{er} values as a function of gel thickness, compared with the corrected modulus $E_{er,c}$ values taking into account the underlying substrate effect: (a) 12.5% PAAm hydrogels (b)20% PAAm hydrogels (one asterisk * denotes $p < 0.001$, two asterisks ** denotes $p > 0.05$).

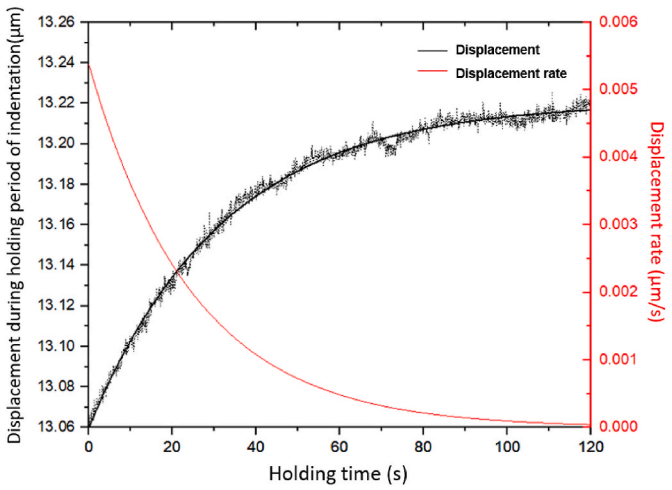

Fig. 5. Typical displacement data curve, fitting curve and displacement rate during the hold period of indentation for 20% PAAm hydrogels with a layer thickness of 27 μm.

independent of δ.

4.3. Effect of confinement on hydraulic conductivity

Fig. 8 shows the K values plotted as a function of α for all the 12.5% and 20% PAAm tested samples. The K values decreased as α increased for both 12.5% and 20% PAAm. The trendlines between the two concentrations of PAAm were almost parallel. The K values of 12.5% PAAm were more than one order of magnitude higher than those of 20% PAAm.

The average and standard deviations of the K for each PAAm specimen are summarised in Table 2. The averaged K values of the 27 μm 12.5% PAAm and 55 μm 20% PAAm gels were significantly lower than those obtained from the thicker gels, indicating the hydraulic conductivity was affected by the geometrical confinement of the gels. The intrinsic permeability κ ($\kappa = \eta \cdot K$) was then determined from the bulk hydraulic permeability (K_B) which were calculated by using the fitting equations ($K = K_B \cdot \exp(-0.958\alpha) + (9 \times 10^{-16})$ and $K = K_B \cdot \exp(-0.948\alpha) + (4 \times 10^{-17})$ for 12.5% and 20% PAAm, respectively). The k values were much closer to each other for the PAAm hydrogels of the same gel composition at different layer thicknesses (Table 2). The averaged k values were 3.78 × 10^{-17} and 4.08 × 10^{-18} m^2 for the 12.5% and 20% PAAm, respectively, within in the range for PAAm gels of similar gel composition (Oyen, 2014).

5. Discussion

5.1. Compared to the Bückle's rule and other models

According to Bückle's rule (Bückle, 1965), the maximum indentation depth should be less than 10% of the film thickness to avoid interference from the underlying substrate, based on Vickers and Berkovich tip testing of hard materials with elastic moduli in the gigapascals (GPa) range (Veprek-Heijman and Veprek, 2015). In the present investigation on soft materials, the nanoindentation depth profiling data showed that the apparent modulus E^* values began to increase as the indentation depth increased when the gel thickness was below a "critical thickness" value (Fig. 4). The equilibrium reduced modulus E_{er} values from 55 μm thick 12.5% PAAm and 27 μm thick 20% PAAm were much higher than the average values obtained from thick gel layers even at indentation depths less than 10% of layer thickness (Fig. 2). And thus, the Bückle's rule did not apply here.

To consider the substrate effect, the relationship between the gel thickness and equilibrium reduced modulus was reconstructed using the normalised modulus values and the dimensionless parameter α to account for the influence of the material's composition and testing geometry (Fig. 3). According to this, the elastic moduli of hydrogels made

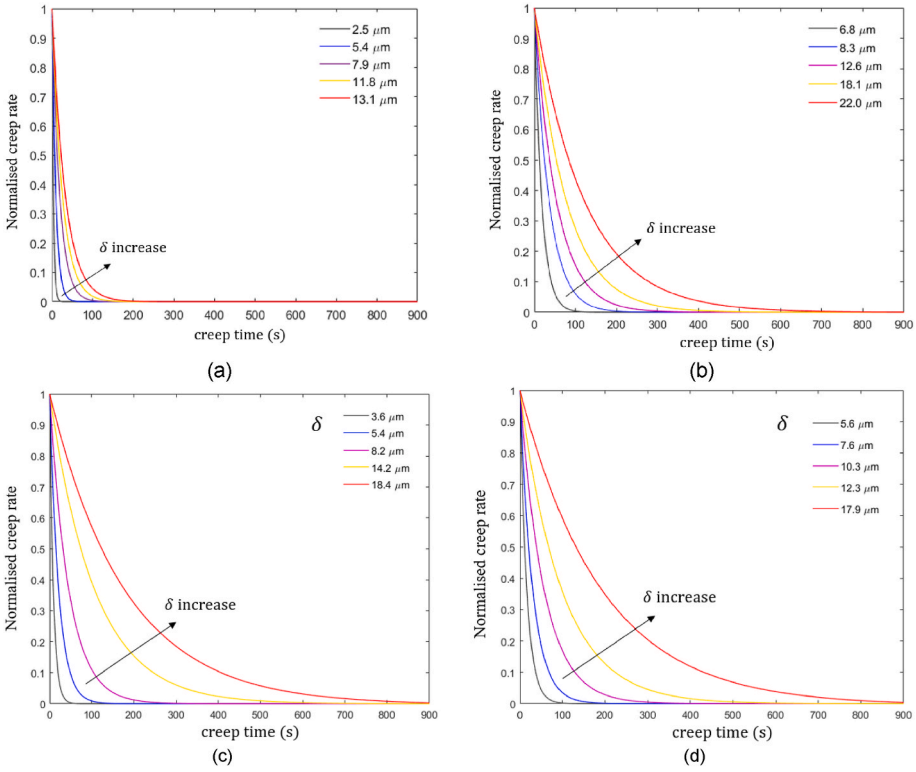

Fig. 6. The normalised creep rate $\dot{\Delta}_c$ as a function of time t for 20% PAAm hydrogels with different indentation depth and hydrogel layer thickness: (a) 27 μm, (b) 215 μm, (c) 277 μm, (d) 555 μm.

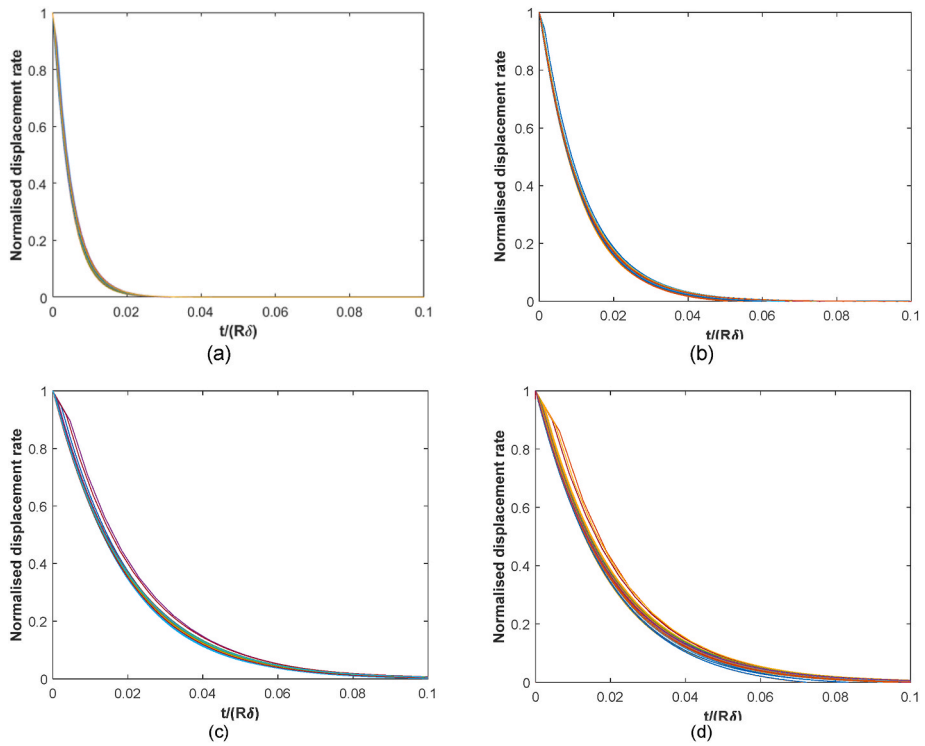

Fig. 7. The normalised creep rate $\dot{\Delta}_c$ as a function of normalised creep time $t/(R\delta)$ for 20% PAAm hydrogels with different indentation depth and hydrogel layer thickness: (a) 27 μm, (b) 215 μm, (c) 277 μm, (d) 555 μm.

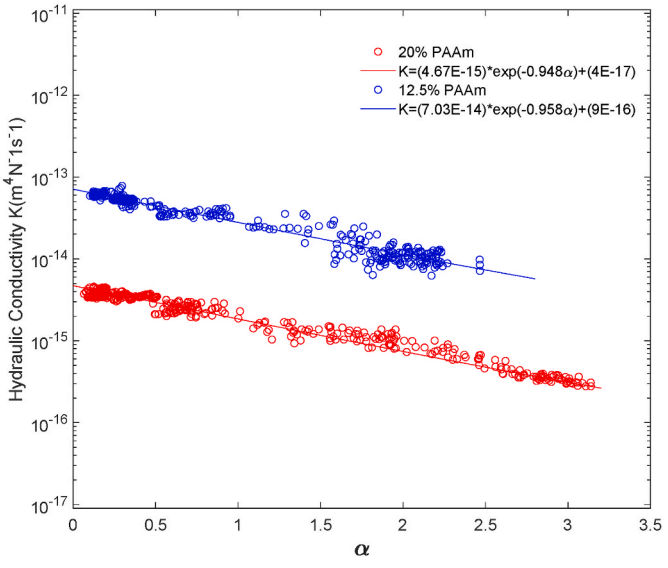

Fig. 8. The effect of confinement α on the hydraulic conductivity K for the 12.5% and 20% PAAm gels with different gel thickness.

from the same materials, but varying thickness were determined, and there was no significant difference in the elastic moduli between thin and thick hydrogel layers (Fig. 4).

As there is no universal rule on the limit of indentation depth, an alternative method could use analytical models to account for the underlying substrate effect on the elastic modulus values. Previous studies have developed analytical models to take into account the substrate effect either by using an integral transformation method (Dimitriadis et al., 2002; Hu et al., 2011) or finite-element analysis (FEA) (Long et al., 2011; Clifford and Seah, 2006b). However, these models have not been validated experimentally, and large discrepancies were found between

Table 2
Average and standard deviations for the apparent hydraulic conductivity K and intrinsic permeability κ

PAAm CONC. (v/v)	Thickness h (μm)	Hydraulic conductivity K ($m^4\ N^{-1}\ s^{-1}$)	Intrinsic permeability κ (m^2)
12.5	54.53 ± 5.74	1.93 ± 0.90 E−14	3.65 ± 1.79 E−17
12.5	308.91 ± 15.55	4.38 ± 2.23 E−14	3.86 ± 1.96 E−17
12.5	596.72 ± 15.78	4.41 ± 1.75 E−14	3.83 ± 1.54 E−17
12.5	781.67 ± 64.93	5.24 ± 0.95 E−14	3.88 ± 1.80 E−17
20	27.44 ± 1.59	2.40 ± 1.41 E−15	4.72 ± 1.93 E−18
20	214.94 ± 52.56	3.60 ± 1.88 E−15	3.81 ± 1.28 E−18
20	276.69 ± 25.17	3.87 ± 2.08 E−15	3.89 ± 1.98 E−18
20	555.49 ± 49.22	4.93 ± 1.96 E−15	4.72 ± 1.87 E−18

those models in Fig. 3 when $\alpha > 1$. The analytical model used by Dimitriadis et al. (2002) predicted a much steeper trend of the normalised E_r against α than the empirical function from the nano-indentation data and the analytical equation by Hu et al. (Kalcioglu et al., 2012) when $\alpha > 1$. This discrepancy can be due to the Poisson's ratio values assumed to be 0.5 for incompressible materials in Dimitriadis et al.'s model (Cha et al., 2010). In this study, this assumption was not applied, and the reduced modulus were reported instead. Hu et al.'s model (Kalcioglu et al., 2012) combined the shear modulus and Poisson's ratio. The empirical function generated in this study agrees well with the analytical equation developed by Hu et al. (Kalcioglu et al., 2012) up to $\alpha \sim 2$ and showed a more visible substrate effect than the Hu et al. model when $\alpha > 2$. Thus, Hu et al.'s model underestimated the substrate effect for highly confined hydrogels ($\alpha > 2$).

5.2. Viscoelasticity vs. poroelasticity

Viscoelasticity and poroelasticity, as time-dependent behaviours, can both exist in hydrogels, and one can dominate the deformation behaviour when testing at different time or length scales. However, few experimental methods are capable of distinguishing and decoupling these behaviours. Previous studies have achieved this by investigating the stress-relaxation process either via indentation tests (Hu et al., 2011) or on a micro-strain tester (Wang et al., 2014). The present study proposes a new method of utilising displacement rate data during holding period of depth profiling indentation, to distinguish the viscoelastic and poroelastic properties of hydrogels.

The results demonstrated that the curves of normalised displacement rate vs. time (t) strongly depend upon the indentation depth (δ) (Fig. 6). The contact areas increase with increased indentation depth, and consequently, the time required to achieve the equilibrium state increased. The viscoelasticity is negligible for the present characterising length and time scale since the curves of normalised creep rate vs. normalised time (t_n) is independent of δ (Fig. 7). The viscoelastic relaxation time is independent of the indentation contact area while the poroelastic relaxation time scales with a^2/D where D is the diffusivity of the gels, and can be given by the permeability as $D = \frac{2G_0k(1-\nu)}{\eta(1-2\nu)}$ (G_0 is the shear modulus) (Wang et al., 2014). As such, the poroelastic behaviour was dominant rather than viscoelastic behaviour for PAAm hydrogels.

5.3. Hydraulic conductivity of poroelastic hydrogels

A poroelastic indentation model was proposed to extract the hydraulic permeability of unconfined ($\alpha < 1$) or moderately confined hydrogels ($1 \leq \alpha \leq 3$). When the thickness decreases and the confinement increase, the flow asymptotes towards a one-dimensional radial flow, assumed by the model in Eqs. (8)–(11), which is similar to an asymptotic solution in the previous studies (Mak et al., 1987; Ateshian et al., 1994). Correspondingly, the hydraulic conductivity should asymptotes towards a constant, which can be seen in the fitting equations listed in Fig. 8. The results also demonstrated that the apparent hydraulic conductivity (Darcy's permeability) of hydrogels would decrease with the confinement of hydrogels, especially for thin hydrogel layers of thickness<200 μm (Fig. 8, Table 2). The calculated K values can differ between thin and thick PAAm gels (Table 2). This indicates that the water migration can be more constrained by the impermeable substrate for thin hydrogel layers as the geometrical confinement increases, which in turn increased the apparent stiffness of the hydrogels.

The results here can be compared with the data reported recently by Lai and Hu (2018) who used AFM-based nanoindentation for the PAAm gels submerged in the polyethylene glycol (PEG) solutions. They measured the shear moduli of 12% PAAm hydrogels in PEG solutions in the range between 3.9 and 9.2 kPa, which were in the same range compared to the $E_{er,c}$ values measured in this study for 12.5% PAAm gels in PBS solution. The diffusivity of the PAAm gels in PEG solutions with different concentrations reported by Lai and Hu (2018) were in the range between 10^{-12} m^2s^{-1} to 10^{-10} m^2s^{-1}, corresponding to an intrinsic permeability κ in the range of 10^{-19} to 10^{-17} m^2, comparable to the values obtained here.

Degen et al. (2020) reported an intrinsic permeability ($\kappa = 1.28 \times 10^{-18}$ m^2) obtained from highly confined polyacrylamide gels, in the similar range, but lower than that of the bulk PAAm materials in this study. They applied a linear relationship between apparent elastic moduli and increased confinement α, similar to Hu et al.'s model (Hu et al., 2011) (Fig. 3). In contrast, an exponential relationship was observed in this study when $\alpha > 1$. A linear relationship would underestimate the influence of the substrate elasticity on the apparent stiffness and subsequently overestimate the influence of the confined fluid flow.

In this study, thin hydrogels exhibited significantly higher apparent stiffness compared to their elastic modulus, attributable to the stiffness of the underlying substrate and constraint fluid flow. This study decoupled these influences and quantified the elastic modulus and intrinsic permeability of thin hydrogel layers using nanoindentation depth profiling and a poroelastic model. Numerous studies have elucidated the influence of the hydrogel stiffness and structure on cell differentiation (Evans and Gentleman, 2014). Cells or groups of cells can 'feel through' thin hydrogels and begin to spread more progressively as the hydrogel gets thinner. In the authors' study (Hernandez-Miranda et al., 2023), it was hypothesised that cell-traction-induced matrix deformations and cellular differentiation can be affected not only by the elastic modulus of the hydrogel substrates but also their geometry. Significant differences were observed in cell behaviour across various hydrogel thicknesses and geometries within the range we investigated here. Moreover, differentiation is subject to changes in the ECM stiffness to differentiate to the specific cell type that matches the tissue stiffness; 0.1–1 kPa hydrogels are neurogenic, 8–17 kPa are myogenic, and 25–40 kPa are osteogenic (Engler et al., 2006). The Young's moduli of soft and stiff PAAm hydrogels investigated here are 5 and 50 kPa respectively, which are comparable to those ranges. These values of mechanical properties of thin PAAm hydrogel layers hold significance in the context of cell culture models and will provide valuable mechanistic insights for the fundamental study of cell mechanobiology.

6. Conclusion

The study presents a depth profiling nanoindentation method for characterising the elastic moduli and hydraulic conductivity of thin, soft hydrogel layers adhered to an impermeable stiff substrate. The proposed method took into account the effects of the underlying substrate, including the presence of a rigid substrate within the interaction volume of the indentation, as well as the impact of fluid flow restriction caused by an impermeable substrate and indenter. Using a combination of Darcy's Law and displacement rate during the holding period of nanoindentation, analytical models were developed to describe poroelastic flow during the holding period that the fluid migrates out of the pressed fluid-filled region of thin and confined hydrogel layers. The elastic moduli and intrinsic permeability of thin PAAm hydrogel layers were determined, and the values were found to be the same as those of thick PAAm hydrogels.

CRediT authorship contribution statement

Dichu Xu: Writing – original draft, Validation, Methodology, Investigation, Formal analysis, Data curation. **Maria Luisa Hernandez Miranda:** Writing – original draft, Resources. **Nicholas D. Evans:** Writing – review & editing, Supervision, Resources, Conceptualization. **Bram G. Sengers:** Writing – review & editing, Supervision. **Martin Browne:** Writing – review & editing, Supervision, Project administration, Funding acquisition. **Richard B. Cook:** Writing – review & editing, Supervision, Project administration, Funding acquisition, Conceptualization.

Declaration of competing interest

The authors declare that they have no known competing financial interests or personal relationships that could have appeared to influence the work reported in this paper.

Data availability

Data will be made available on request.

Acknowledgements

This work was supported by funding from the European Union (EU) within its Horizon 2020 programme, project MDOT (Grant Agreement

814654). MHM and NDE acknowledge CONAHCyT (National Council of humanities, Sciences and Technologies), Mexico and the Faculty of Medicine, Southampton University, UK, for funding.

References

Asp, M.E., Ho Thanh, M.-T., Germann, D.A., Carroll, R.J., Franceski, A., Welch, R.D., Gopinath, A., Patteson, A.E., 2022. Spreading rates of bacterial colonies depend on substrate stiffness and permeability. PNAS Nexus 1 (1), pgac025. https://doi.org/10.1093/pnasnexus/pgac025.

Ateshian, G.A., Lai, W.M., Zhu, W.B., Mow, V.C., 1994. An asymptotic solution for the contact of two biphasic cartilage layers. J. Biomech. 27 (11), 1347–1360. https://doi.org/10.1016/0021-9290(94)90044-2.

Bear, J., 1988. Dynamics of Fluids in Porous Media. Courier Corporation.

Biot, M.A., 1955. Theory of elasticity and consolidation for a porous anisotropic solid. J. Appl. Phys. 26 (2), 182–185. https://doi.org/10.1063/1.1721956.

Bückle, H., 1965. Mikrohärteprüfung Und Ihre Anwendung. Berliner Union.

Buxboim, A., Rajagopal, K., Brown, A.E.X., Discher, D.E., 2010. How deeply cells feel: methods for thin gels. J. Phys. Condens. Matter 22 (19). https://doi.org/10.1088/0953-8984/22/19/194116.

Cao, K., Flegg, D.S., Lin, S., Lagugné-Labarthet, F., Mequanint, K., Gillies, E.R., 2019. Fabrication and in situ cross-linking of carboxylic-acid-functionalized poly(ester amide) scaffolds for tissue engineering. ACS Appl. Polym. Mater. 1 (9), 2360–2369. https://doi.org/10.1021/acsapm.9b00475.

Cha, C., Kim, S.Y., Cao, L., Kong, H., 2010. Decoupled control of stiffness and permeability with a cell-encapsulating poly(ethylene glycol) dimethacrylate hydrogel. Biomaterials 31 (18), 4864–4871. https://doi.org/10.1016/j.biomaterials.2010.02.059.

Chan, E.P., Deeyaa, B., Johnson, P.M., Stafford, C.M., 2012a. Poroelastic relaxation of polymer-loaded hydrogels. Soft Matter 8 (31), 8234–8240. https://doi.org/10.1039/c2sm25363a.

Chan, E.P., Hu, Y., Johnson, P.M., Suo, Z., Stafford, C.M., 2012b. Spherical indentation Testin.g of poroelastic relaxations in thin hydrogel layers. Soft Matter 8 (5), 1492–1498. https://doi.org/10.1039/c1sm06514a.

Chan, E.P., Hu, Y., Johnson, P.M., Suo, Z., Stafford, C.M., 2012c. Spherical indentation testing of poroelastic relaxations in thin hydrogel layers. Soft Matter 8 (5), 1492–1498. https://doi.org/10.1039/c1sm06514a.

Chau, A.L., Cavanaugh, M.K., Chen, Y.T., Pitenis, A.A., 2021. A simple contact mechanics model for highly strained aqueous surface gels. Exp. Mech. 61 (4), 699–703. https://doi.org/10.1007/s11340-021-00699-5.

Chaudhuri, O., Gu, L., Klumpers, D., Darnell, M., Bencherif, S.A., Weaver, J.C., Huebsch, N., Lee, H.P., Lippens, E., Duda, G.N., Mooney, D.J., 2016. Hydrogels with tunable stress relaxation regulate stem cell fate and activity. Nat. Mater. 15 (3), 326–334. https://doi.org/10.1038/nmat4489.

Chen, J., Bull, S.J., 2009. On the factors affecting the critical indenter penetration for measurement of coating hardness. Vacuum 83 (6), 911–920. https://doi.org/10.1016/j.vacuum.2008.11.007.

Clifford, C.A., Seah, M.P., 2006a. Modelling of nanomechanical nanoindentation measurements using an AFM or nanoindenter for compliant layers on stiffer substrates. Nanotechnology 17 (21), 5283–5292. https://doi.org/10.1088/0957-4484/17/21/001.

Clifford, C.A., Seah, M.P., 2006b. Modelling of nanomechanical nanoindentation measurements using an AFM or nanoindenter for compliant layers on stiffer substrates. Nanotechnology 17 (21), 5283–5292. https://doi.org/10.1088/0957-4484/17/21/001.

Clifford, C.A., Seah, M.P., 2009. Nanoindentation measurement of Young's modulus for compliant layers on stiffer substrates including the effect of Poisson's ratios. Nanotechnology 20 (14). https://doi.org/10.1088/0957-4484/20/14/145708.

Cushing, M.C., Anseth, K.S., 2007. Hydrogel cell cultures. Science 316 (5828), 1133–1134. https://doi.org/10.1126/science.1140171.

Degen, G.D., Chen, Y.T., Chau, A.L., Månsson, L.K., Pitenis, A.A., 2020. Poroelasticity of highly confined hydrogel films measured with a surface forces apparatus. Soft Matter 16 (35), 8096–8100. https://doi.org/10.1039/d0sm01312a.

Delavoipière, J., Tran, Y., Verneuil, E., Chateauminois, A., 2016. Poroelastic indentation of mechanically confined hydrogel layers. Soft Matter 12 (38), 8049–8058. https://doi.org/10.1039/c6sm01448h.

Dimitriadis, E.K., Horkay, F., Maresca, J., Kachar, B., Chadwick, R.S., 2002. Determination of elastic moduli of thin layers of soft material using the atomic force microscope. Biophys. J. 82 (5), 2798–2810. https://doi.org/10.1016/S0006-3495(02)75620-8.

Engler, A.J., Sen, S., Sweeney, H.L., Discher, D.E., 2006. Matrix elasticity directs stem cell lineage specification. Cell 126 (4), 677–689. https://doi.org/10.1016/j.cell.2006.06.044.

Evans, N.D., Gentleman, E., 2014. The role of material structure and mechanical properties in cell–matrix interactions. J. Mater. Chem. B 2 (17), 2345. https://doi.org/10.1039/c3tb21604g.

Evans, N., Minelli, C., Gentleman, E., LaPointe, V., Patankar, S., Kallivretaki, M., Chen, X., Roberts, C., Stevens, M., 2009. Substrate stiffness affects early differentiation events in embryonic stem cells. Eur. Cell. Mater. 18, 1–14. https://doi.org/10.22203/eCM.v018a01.

Fu, M., Liang, Y., Lv, X., Li, C., Yang, Y.Y., Yuan, P., Ding, X., 2021. Recent advances in hydrogel-based anti-infective coatings. J. Mater. Sci. Technol. 85, 169–183. https://doi.org/10.1016/j.jmst.2020.12.070.

Galli, M., Oyen, M.L., 2008. Spherical indentation of a finite poroelastic coating. Appl. Phys. Lett. 93 (3) https://doi.org/10.1063/1.2957993.

Galli, M., Oyen, M.L., 2009. Fast identification of poroelastic parameters from indentation tests. CMES - Comput. Model. Eng. Sci. 48 (3), 241–269. https://doi.org/10.3970/cmes.2009.048.241.

Hernandez Miranda, M.L., 2023. Individual and Collective Mechanosensing of Extracellular Matrix Thickness in Skeletal Stem Cell Differentiation. Doctoral dissertation, University of Southampton.

Hu, Y., Zhao, X., Vlassak, J.J., Suo, Z., 2010. Using indentation to characterize the poroelasticity of gels. Appl. Phys. Lett. 96 (12) https://doi.org/10.1063/1.3370354.

Hernandez-Miranda, M., Xu, D., Johnston, D.A., Browne, M., Cook, R.B., Sengers, B.G., Evans, N.D., 2023. Geometric constraint of mechanosensing in bone marrow stromal cell cultures prevents stiffness-induced differentiation. Available on bioRxiv. https://doi.org/10.1101/2023.10.05.560162.

Hu, Y., Chan, E.P., Vlassak, J.J., Suo, Z., 2011. Poroelastic relaxation indentation of thin layers of gels. J. Appl. Phys. 110 (8), 108–111. https://doi.org/10.1063/1.3647758.

Huang, H., Tan, Y., Ayers, D.C., Song, J., 2018. Anionic and zwitterionic residues modulate stiffness of photo-cross-linked hydrogels and cellular behavior of encapsulated chondrocytes. ACS Biomater. Sci. Eng. 4 (5), 1843–1851. https://doi.org/10.1021/acsbiomaterials.8b00124.

Islam, M.R., Oyen, M.L., 2021. A poroelastic master curve for time-dependent and multiscale mechanics of hydrogels. J. Mater. Res. https://doi.org/10.1557/s43578-020-00090-5.

Kalcioglu, Z.I., Mahmoodian, R., Hu, Y., Suo, Z., Van Vliet, K.J., 2012. From macro- to microscale poroelastic characterization of polymeric hydrogels via indentation. Soft Matter 8 (12), 3393–3398. https://doi.org/10.1039/c2sm06825g.

Kontomaris, S.V., Malamou, A., 2020. Hertz model or oliver & pharr analysis? Tutorial regarding AFM nanoindentation experiments on biological samples. Mater. Res. Express 7 (3). https://doi.org/10.1088/2053-1591/ab79ce.

Lai, Y., Hu, Y., 2018. Probing the swelling-dependent mechanical and transport properties of polyacrylamide hydrogels through AFM-based dynamic nanoindentation. Soft Matter 14 (14), 2619–2627. https://doi.org/10.1039/c7sm02351k.

Li, J., Mooney, D.J., 2016. Designing hydrogels for controlled drug delivery. Nat. Rev. Mater. 1 (12), 1–17. https://doi.org/10.1038/natrevmats.2016.71.

Long, R., Hall, M.S., Wu, M., Hui, C.Y., 2011. Effects of gel thickness on microscopic indentation measurements of gel modulus. Biophys. J. 101 (3), 643–650. https://doi.org/10.1016/j.bpj.2011.06.049.

Mak, A.F., Lai, W.M., Mow, V.C., 1987. Biphasic indentation of articular cartilage—I. Theoretical analysis. J. Biomech. 20 (7), 703–714. https://doi.org/10.1016/0021-9290(87)90036-4.

Manika, I., Maniks, J., 2008. Effect of substrate hardness and film structure on indentation depth criteria for film hardness testing. J. Phys. Appl. Phys. 41 (7) https://doi.org/10.1088/0022-3727/41/7/074010.

Munevar, S., Wang, Y.L., Dembo, M., 2001. Traction force microscopy of migrating normal and H-ras transformed 3T3 fibroblasts. Biophys. J. 80 (4), 1744–1757. https://doi.org/10.1016/S0006-3495(01)76145-0.

Nicodemus, G.D., Bryant, S.J., 2008. Cell encapsulation in biodegradable hydrogels for tissue engineering applications. Tissue Eng. - Part B Rev. 14 (2), 149–165. https://doi.org/10.1089/ten.teb.2007.0332.

Oyen, M.L., 2005. Spherical indentation creep following ramp loading. J. Mater. Res. 20 (8), 2094–2100. https://doi.org/10.1557/JMR.2005.0259.

Oyen, M.L., 2008. Poroelastic nanoindentation responses of hydrated bone. J. Mater. Res. 23 (5), 1307–1314. https://doi.org/10.1557/jmr.2008.0156.

Oyen, M.L., 2014. Mechanical characterisation of hydrogel materials. Int. Mater. Rev. 59 (1), 44–59. https://doi.org/10.1179/1743280413Y.0000000022.

Oyen, M.L., Bembey, A.K., Bushby, A.J., 2006. Poroelastic indentation analysis for hydrated biological tissues. Mater. Res. Soc. Symp. Proc. 975, 122–127. https://doi.org/10.1557/proc-975-0975-dd07-05.

Pelham, JR., Wang, Y.L., 1997. Cell locomotion and focal adhesions are regulated by substrate flexibility. Proc. Natl. Acad. Sci. USA 94 (25), 13661–13665. https://doi.org/10.1073/pnas.94.25.13661.

Pereira, D.G., Afonso, A., Medeiros, F.M., 2015. Overview of friedman's test and post-hoc analysis. Commun. Stat. Simulat. Comput. 44 (10), 2636–2653. https://doi.org/10.1080/03610918.2014.931971.

Qian, L., Zhao, H., 2018. Nanoindentation of soft biological materials. Micromachines 9 (12). https://doi.org/10.3390/mi9120654.

Rice, M.A., Anseth, K.S., 2004. Encapsulating chondrocytes in copolymer gels: bimodal degradation kinetics influence cell phenotype and extracellular matrix development. J. Biomed. Mater. Res., Part A 70 (4), 560–568. https://doi.org/10.1002/jbm.a.30106.

Swain, M.V.A., Nohava, J., Eberwein, P.A., 2017. Simple basis for determination of the modulus and hydraulic conductivity of human ocular surface using nano-indentation. Acta Biomater. 50, 312–321. https://doi.org/10.1016/j.actbio.2016.12.007.

Trepat, X., Wasserman, M.R., Angelini, T.E., Millet, E., Weitz, D.A., Butler, J.P., Fredberg, J.J., 2009. Physical forces during collective cell migration. Nat. Phys. 5 (6), 426–430. https://doi.org/10.1038/nphys1269.

Tsou, Y.H., Khoneisser, J., Huang, P.C., Xu, X., 2016. Hydrogel as a bioactive material to regulate stem cell fate. Bioact. Mater. 1 (1), 39–55. https://doi.org/10.1016/j.bioactmat.2016.05.001.

Tusan, C.G., Man, Y.H., Zarkoob, H., Johnston, D.A., Andriotis, O.G., Thurner, P.J., Yang, S., Sander, E.A., Gentleman, E., Sengers, B.G., Evans, N.D., 2018. Collective cell behavior in mechanosensing of substrate thickness. Biophys. J. 114 (11), 2743–2755. https://doi.org/10.1016/j.bpj.2018.03.037.

Veprek-Heijman, M.G.J., Veprek, S., 2015. The deformation of the substrate during indentation into superhard coatings: Bückle's rule revised. Surf. Coat. Technol. 284, 206–214. https://doi.org/10.1016/j.surfcoat.2015.10.064.

Wang, Q.M., Mohan, A.C., Oyen, M.L., Zhao, X.H., 2014. Separating viscoelasticity and poroelasticity of gels with different length and time scales. Acta Mech. Sin. Xuebao 30 (1), 20–27. https://doi.org/10.1007/s10409-014-0015-z.

Xu, D., Harvey, T., Begiristain, E., Domínguez, C., Sánchez-Abella, L., Browne, M., Cook, R.B., 2022. Measuring the elastic modulus of soft biomaterials using nanoindentation. J. Mech. Behav. Biomed. Mater. 133, 105329. https://doi.org/10.1016/j.jmbbm.2022.105329.